MECHANICAL PROPERTIES AND MICROSTRUCTURE OF A TRANSFORMATION INDUCED PLASTICITY STEEL FRICTION STIR SPOT WELDED

Cíntia Cristiane Petry Mazzaferro, cintia.mazzaferro@ufrgs.br
José Antônio Esmerio Mazzaferro, mazza@ufrgs.br
Universidade Federal do Rio Grande do Sul-UFRGS, DEMEC, Porto Alegre, Brazil
Jorge Fernandez dos Santos, jorge.dos.santos@hzg.de
Helmholtz-Zentrum Geesthacht, Institute of Materials Research/Solid State Joining Processes, Geesthacht, Germany
Telmo Roberto Strohaecker, telmo@demet.ufrgs.br
Universidade Federal do Rio Grande do Sul-UFRGS, DEMET, PPGEM, Porto Alegre, Brazil

Abstract. Friction stir spot welding was performed in transformation induced plasticity steel sheets coated with zinc. The joints were produced using rotational speed of 2400 rpm and dwell time of 3 s. Process outputs, microstructures, microhardness and lap-shear tests were investigated. After processing, three different zones were formed in the joints. Final microstructures and hardness in each zone were related to the welding condition used. The zone with highest hardness level was the stir zone, situated near the keyhole left by the pin. Martensite formation took place in this zone. However, allotriomorphic ferrite was also observed in stir zone. Due to the material flow, the formation of a zinc line in stir zone was observed. The fracture of the samples in lap-shear tests occurred following this zinc line, and the microstructure played a second role during fracture.

Keywords: friction stir spot welding, transformation induced plasticity steel

1. INTRODUCTION

Friction stir welding (FSW) is a solid state welding process invented by The Welding Institute in 1991 (Thomas *et al.* 1991). It has been widely used for welding soft materials such as aluminum and magnesium alloys since then. In FSW the pin at the bottom of a rotating cylindrical tool is plunged into workpieces and traversed along the joint to be welded. Welding is achieved by plastic flow of frictionally heated material from ahead of the pin to behind it. The major variant of this process is friction stir spot welding (FSSW). The rotating tool is plunged into workpieces but without being traversed along any direction, as illustrated in Fig. 1 (Mazzaferro 2008). Welding is achieved by plastic flow of frictionally heated material around the pin, in stirring stage. After the tool is withdrawn, a keyhole is left in the workpiece. FSSW can be used in place of single point conventional joining techniques in many applications. For example, Mazda has replaced resistance spot welding and riveting for FSSW in Mazda RX8 passenger (Mazda 2003) and Mazda MX-5 sport (Mazda 2005) cars.
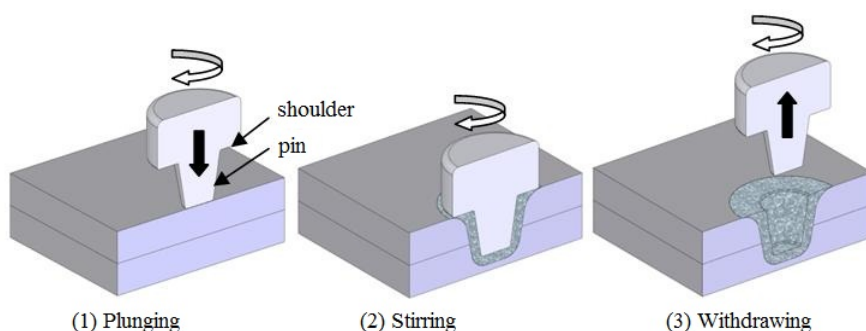
Figure 1. Friction stir spot welding: stages. (Adapted from Mazzaferro, 2008)

Advanced high strength steels (AHSS), which include transformation-induced plasticity (TRIP) steels, were developed for automotive applications to meet the requirements of higher passengers safety, weight reduction and decrease of fuel consumption. There is an increasing interest concerning the application of TRIP steels in automotive industry because they can provide an excellent combination of strength, formability and energy absorption. The microstructure of TRIP steels is obtained by alloying, usually with C, Mn and Si, and a two-stepped heat treatment, resulting in ferrite, bainite and retained austenite (Jacques *et al.* 2001a, Skálová *et al.* 2006). When these steels are subjected to deformation, the retained austenite can transform into martensite, which delays the onset of necking resulting in high work-hardening and high total elongation (Srivastava *et al.* 2007, Chung *et al.* 2010).

Some studies concerning AHSS showed the feasibility of obtaining joints with good mechanical properties using FSSW (Feng *et al.* 2005, Kyffin *et al.* 2006a, Kyffin *et al.* 2006b, Khan *et al.* 2007, Santella *et al.* 2010). However, these studies did not include TRIP steels.

The purpose of this paper is to investigate the friction stir spot welding of a TRIP 800 steel. Process characteristics, microstructural development and mechanical response were evaluated using a rotational speed of 2400 rpm and a dwell time of 3 s.

2. EXPERIMENTAL PROCEDURE

The experimental material was a commercial sheet of TRIP 800 with thickness of 1.0 mm and chemical composition 0.19C – 1.55Mn – 1.65Si – 0.039 Al – 0.016P – 0.0009S (wt. %). This steel was cold-rolled and electrogalvanized. The zinc coating layer was about 7.5μm on both sides.

FSSW was performed in a Gantry Welding Machine using displacement control, with the tool plunging to a pre-determined maximum depth (1.6 mm in this study) before applying dwell time. The welds were carried out using a polycrystalline cubic boron nitride (PCBN) tool, which had a concave shoulder with diameter of 15mm, a conic pin with minimum diameter of 5 mm and a 1.5 mm length pin featuring six equally spaced flats. Friction stir spot welds were produced with fixed plunge rate of 0.1 mm/s, tool rotational speed of 2400 rpm and dwell time of 3 seconds. Axial forces and torque, as well as tool displacement, were measured and logged on a desktop computer.

After metallographic preparation according to the procedure developed by Mazzaferro (2008), the joints were evaluated via optical microscope (OM) Leica DM IMR using LePera etching, and scanning electron microscope (SEM) Zeiss DSM 962 using Nital 1% as etchant. LePera is a colored tint etching reagent. According with literature (Girault *et al.* 1998) after etching ferrite appears blue-green, bainite is brown and both retained austenite and martensite are white.

The volume fraction and carbon content of retained austenite were measured by X-ray diffractometry using Co-K$_\alpha$ radiation. A step scan within the 2θ interval between 45° and 120° at 0.05^o was done. Integrated intensities of diffraction peaks (111)$_\gamma$, (200)$_\gamma$, (220)$_\gamma$ e (311)$_\gamma$ and (110)$_\alpha$, (200)$_\alpha$ e (211)$_\alpha$ were calculed, and the volume fraction of retained austenite, and ferrite, bainite and martensite was calculated according to direct comparison method. The carbon content in retained austenite was calculated using the empirical expression *a$_0$ = 3.578 + 0.033(%C)* (Jacques et al. 2001b), where *a$_0$* is the lattice constant of retained austenite in Å from (111)$_\gamma$ peak and *%C* is the carbon content of retained austenite.

Vickers microhardness testing was performed in a Zwick Roell Identec ZHV machine. The testing was carried out on transverse cross sections as a function of position from the weld center line and at a distance of 0.70 mm from upper sheet surface. The load during hardness testing was 0.5 kg with a 0.25 mm pitch distance between measurements, and was applied during 10 s.

Joint mechanical properties were evaluated by measuring the peak fracture load during lap-shear testing at a loading rate of 0.1 mm/s in a Zwick Roell 1484 machine. The specimens had dimensions 45 mm wide and 175 mm long and the weld was centered at the overlap (35mm) as specified in ISO 14273 (2000). Three samples were tested, and the surface fractures of each sample were observed using SEM. After the analyses of the fractures, the samples were cut in the direction of applied load in shear tests and analysed in OM and SEM, using Nital 1% as etchant.

3. RESULTS AND DISCUSSION

3.1. Process outputs

Axial force, torque and plunging depth (tool displacement) outputs are showed in Fig.2. When the pin touches the surface of the upper sheet, due to the material resistance against deformation, force and torque start to increase, until the force reaches the F1 value in Fig. 2. As pin penetration continues, the temperature increases due to the frictional heating and the material plasticizes; its resistance decreases and there is a drop in the force value. The tool axial displacement causes the upwards movement of the material, like a reverse extrusion. When the shoulder touches this extruded material, force and torque values increase again due to the "forging force" produced by the shoulder. Immediately before the dwell period, where the tool remains rotating but there is no axial displacement, the force reaches another peak represented by F2 in Fig. 2 and the torque reaches its maximum value. During dwell time there is a drop in force and torque values because of the low resistance of the material beeing deformed, due to the frictional heating.
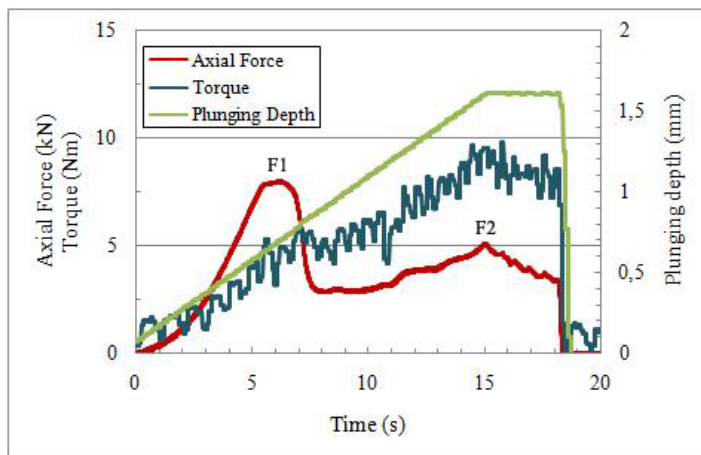
Figure 2. Axial force, torque and plunging depth outputs during FSSW of theTRIP 800 steel.

The energy delivered during FSSW depends on axial force, penetration depth, tool rotational speed and torque. Plunge rate is another factor that indirectly affects energy (Su *et al.* 2005). Usually, higher heat inputs lead to greater stir zone extensions (Su *et al.* 2006a, Gerlich *et al.* 2005). The heat input was calculated using Eq. (1) (Su *et al.* 2005):

$$Energy\ input = \sum_{n=1}^{n=N} Force(n).(x_n - x_{n-1}) + \sum_{n=1}^{n=N} Torque(n).\omega(n).\Delta t \qquad (1)$$

where x_n is the tool penetration depth at moment n, ω is the angular velocity (rad/s), Δt is the acquisition time increment (s) and N is the total number of time increments considered.

Usually, higher heat inputs lead to greater stir zone extensions (Su *et al.* 2006a, Gerlich *et al.* 2005). The energy generated during FSSW creates the stir zone and the excess energy dissipates in the sheets being welded, in the tool assembly, anvil support, and clamp and surrounding atmosphere (Su *et al.* 2006b).

The average heat input for the joints produced in this study was (23.97 ± 0.92) kJ. There is no previous studies concerning the FSSW of TRIP to compare to this value. However, compared to results from FSSW of different materials (Su *et al.* 2005, Gerlich *et al.* 2005, Su *et al.* 2006a, Su *et al.* 2006b, Khan *et al.* 2007), the calculated energy input here is quite high. This can be attributed mainly to the low plunge rate used, which was 0.1 mm/s.

3.2. Microstructures

Figure 3 shows the microstructure of the TRIP steel. It is composed by dispersed bainitic ferrite and retained austenite in a soft ferritic matrix.
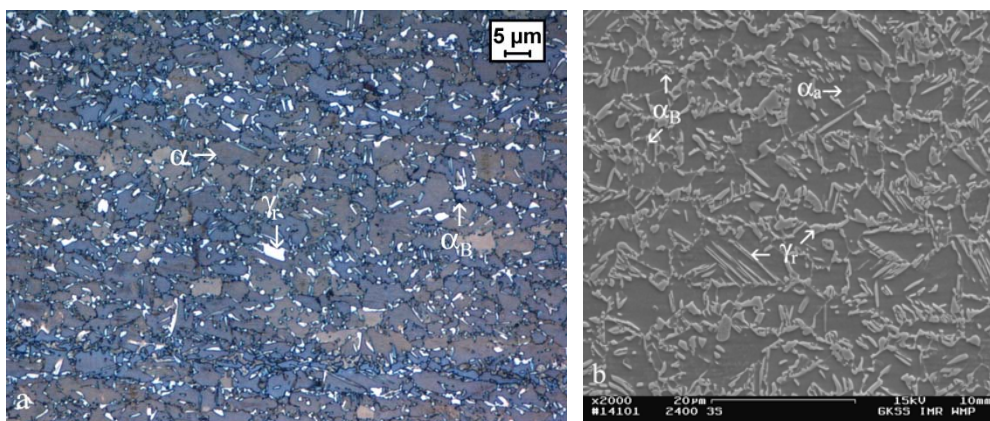
Figure 3. Microstructure of the TRIP 800 steel: (a) OM; (b) SEM. α=ferrite; α$_B$=bainitic ferrite; γ$_r$=retained austenite.

As a result of thermal cycles and deformation imposed by the FSSW process, three different zones were formed in the joints, as can be observed in Fig. 4(a): stir zone (SZ), where the reached temperature and intense plastic deformation leads to the mechanical mixing of upper and lower sheets, as well as microstructural transformations; thermomechanically affected zone (TMAZ), characterized by high temperature peak coupled with moderate plastic deformation (notice that due to deformation, there is no a defined limit between SZ and TMAZ; the transition between

these zones is gradual) ; and heat affected zone (HAZ), which does not experience plastic deformation. The HAZ can be divided into two subzones, HAZ1 and HAZ2, where different microstructural changes occurred due to the thermal gradient. Some information about the material flow is presented in Fig. 4(b): it is possible to identify the material flow adjacent to the keyhole and the material flow caused by the shoulder movement, at top left. Gerlich *et al.* (2008) suggested that in FSSW there is the movement of upper sheet material from the location beneath the tool shoulder and lower sheet material from the bottom of the rotating pin towards the top of the rotating pin in a spiral movement. Notice in Fig. 4(b) that the interface between the sheets, coated by zinc, is also visible, but there is a certain point where this interface does not exist anymore and, instead of it, a fine zinc line formed by the material flow can be seen.
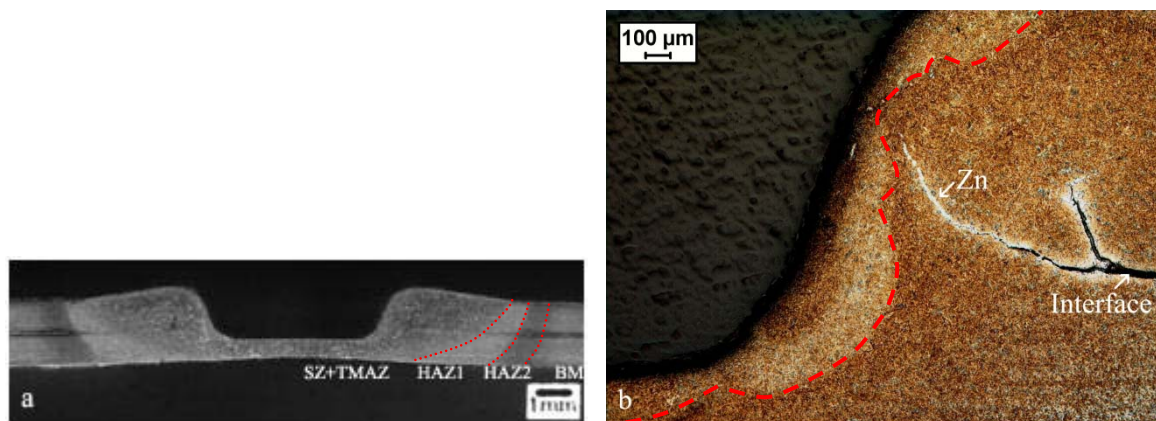
Figure 4. (a) Optical macrograph showing the different zones formed after FSSW: SZ, TMAZ and HAZ (BM is the base material). Etching Nital 2%; (b) close view of the region near the keyhole left by the pin. Here, the material flow is emphasized by the traced line. OM.

The resultant microstructure in SZ can be observed in Fig. 5. The formation of allotriomorphic ferrite (α_a), Widmanstätten ferrite (α_W), upper bainite (B_U), coalesced bainite (B_C), martensite (M) and martensite-austenite constituent (MA), indicate that the temperature during heating was above Ac3, and the cooling rate was slower than the critical for obtaining 100% martensitic microstructures. Gould *et al.* (2006) calculated this cooling rate for a TRIP with similar chemical composition as 45°C/s. In FSSW process, microstructural transformations from austenitic field are influenced by two concurrent factors: deformation and cooling rate. Faster cooling rates contribute to the formation of displacive products, like Widmanstätten ferrite, bainite and martensite, because there is not enough time for carbon diffusion. However, an increase in deformation causes the allotriomorphic ferrite formation, due to the increase in austenite grain boundaries (Bhadeshia 1995, Hanlon *et al.* 2001, Ryu *et al.* 2002) and/or reduction in the undercooling necessary for its nucleation (Hong *et al.* 2003, Liu *et al.* 1995). In this study, the welding parameters selected caused a large amount of allotriomorphic ferrite formed in the region near the keyhole left by the pin, as can be seen in Fig. 6, probably by the conjugated effect of slow cooling rate (due to the high heat input) and large deformation.
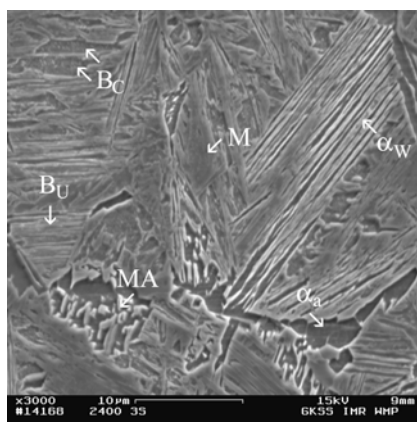
Figure 5. Microstructure in SZ: α_a=allotriomorphic ferrite; α_W=Widmanstätten ferrite; B_C= coalesced bainite; B_U= upper bainite; M=martensite; MA=martensite-austenite constituent. SEM.
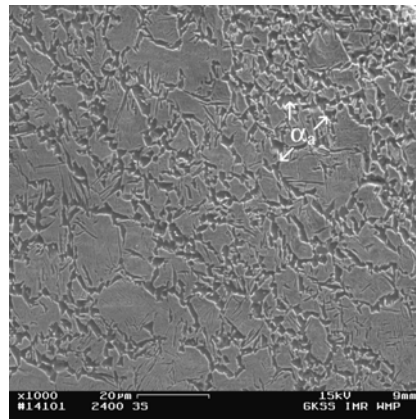
Figure 6. Allotriomorphic ferrite (α_a) formed in SZ. For reference, the keyhole left by the pin is at right.

During cooling, formation of coalesced bainite begins at the austenite grain boundary. It develops into a coarse feature through the coalescence of independently nucleated platelets which are in the same crystallographic orientation. This happens when the bainite formation temperature is close to the martensite start temperature. Several authors (Larn and Yang 2000, Jandová *et al.* 2004, Kaputkina *et al.* 1986) suggested that deformation decreases bainite formation temperature. So in the present study coalesced bainite formation can be attributed to the deformation imposed by the process, for forming large amounts of platelets with same orientation, and/or for decreasing the bainite formation temperature. It is possible that the formation of martensite-austenite constituent (MA) has been facilitated by the large amount of allotriomorphic ferrite. As the carbon solubility in ferrite is quite low, there is an enrichment of the adjacent austenite with this element and with subsequent cooling, when the M_S temperature is reached, formation of MA occurs.

The SZ, mainly in the region near the keyhole, is the zone where higher deformation and temperature are expected. As pancake-shaped grains were no observed, is believed that deformation processes took place in temperatures above the non-recrystallization temperature of this steel, which was 910°C for a TRIP with similar chemical composition (Hanzaki *et al.* 1997).

The resultant microstructure composed by ferrite, austenite, bainite and martensite in TMAZ, in Fig. 7, indicates that the material was heated to peak temperature within the intercritical temperature range (between Ac1-Ac3), where ferrite and austenite coexist. During cooling, some austenite grains transformed into bainite and martensite, but mainly the larger ones, probably due to the chemical stabilization of the austenite: smaller grains have lower carbon content and then their MS temperatures are lower. Moreover, the microstructure in TMAZ seems to be lightly deformed as a result of moderate deformation imposed by the process in this zone, so this can have contributed to the mechanical stabilization of the austenite: grains with higher dislocation densities have higher stacking fault energy, resulting in lower driving-force for martensitic transformation (Wan *et al.* 2003, Whelan *et al.* 1957). Table 1 shows the volume fraction of retained austenite in TMAZ, as well as in BM for comparison. As revealed by micrographs, significant amount of retained austenite was transformed due to temperature/deformation cycle in this zone.
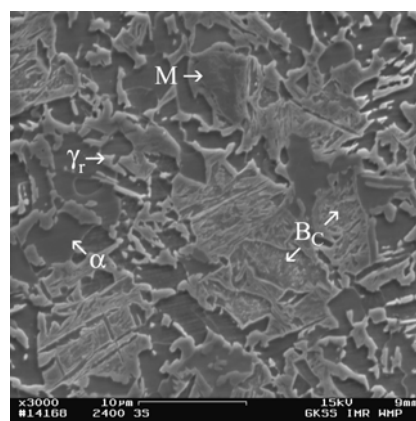
Figure 7. Microestructure in TMAZ: α=ferrite; B_C= coalesced bainite; M=martensite; γ_r=retained austenite. SEM.

Table 1. Volume fraction of retained austenite γ_r and its carbon content for TMAZ. For comparison, the values for the base material, before welding, are also shown.

TMAZ		BM	
%γ_r	%C	%γ_r	%C
9.22	0.89	16.83	1.06

In HAZ1, similarly to TMAZ, the reached temperature formed a mixture of austenite and ferrite during heating. However, in this subzone the microstructure was not affected by deformation. After cooling, the resultant microstructure was composed mainly by ferrite and retained austenite, Fig. 8(a). The temperature in HAZ2 was probably lower than Ac1. In this subzone, as can be observed in Fig. 8(b), partial transformation of austenite into bainitic ferrite took place. This can be attributed to the slow cooling rate for the welding condition used in this study, and the exposure of the material to the temperature range of bainitic transformation. This result is in agreement with studies of Jacques *et al.* (2007) and Zaefferer *et al.* (2004) where higher bainitic ferrite fractions transformed by increasing temperature or time of isothermal treatment. The volume fraction of retained austenite for these zones is shown in Tab. 2. Notice that carbon content of retained austenite in HAZ2 is higher than that one in HAZ1. The maximum solubility of carbon in bainitic ferrite is about 0.4% (Samek et al. 2006), so whereas bainitic ferrite grows, there is a rejection of the exceeded carbon to the surrounding austenite.
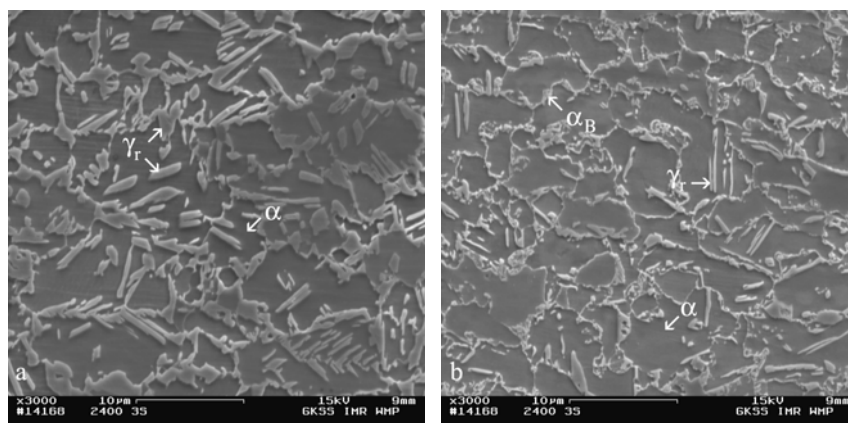
Figure 8. Microstructure in (a) HAZ1; (b) HAZ2. α=ferrite; α$_B$=bainitic ferrite; γ$_r$=retained austenite. SEM.

Table 2. Volume fraction of retained austenite γ$_r$ and its carbon content for HAZ1 and HAZ2. For comparison, the values for the base material, before welding, are also shown.

HAZ1		HAZ2		BM	
%γ_r	%C	%γ_r	%C	%γ_r	%C
8.53	0.64	8.04	0.96	16.83	1.06

3.3. Mechanical Properties

Microhardness profile of a FSSW joint can be observed in Fig. 9. In this figure is also indicated the approximated size of the different zones formed during FSSW. Near the keyhole left by the pin, corresponding to the beginning of SZ, there is a large hardness variation, caused by indentations in areas with large amounts of ferrite (lower hardness) or in areas with large amounts of bainite and/or martensite. In SZ, the maximum hardness value was about 480 HV. From this zone, there was a gradual drop in hardness values until HAZ2 is reached. As demonstrated through nanohardness testing in TRIP steels (Furnémont *et al.* 2002) the austenite is harder than bainitic ferrite and, as expected, than ferrite. HAZ2 is characterized by presenting lower amount of retained austenite, but larger amount of bainitic ferrite, than BM. Because of this, there was a small softening in HAZ2 compared to BM.
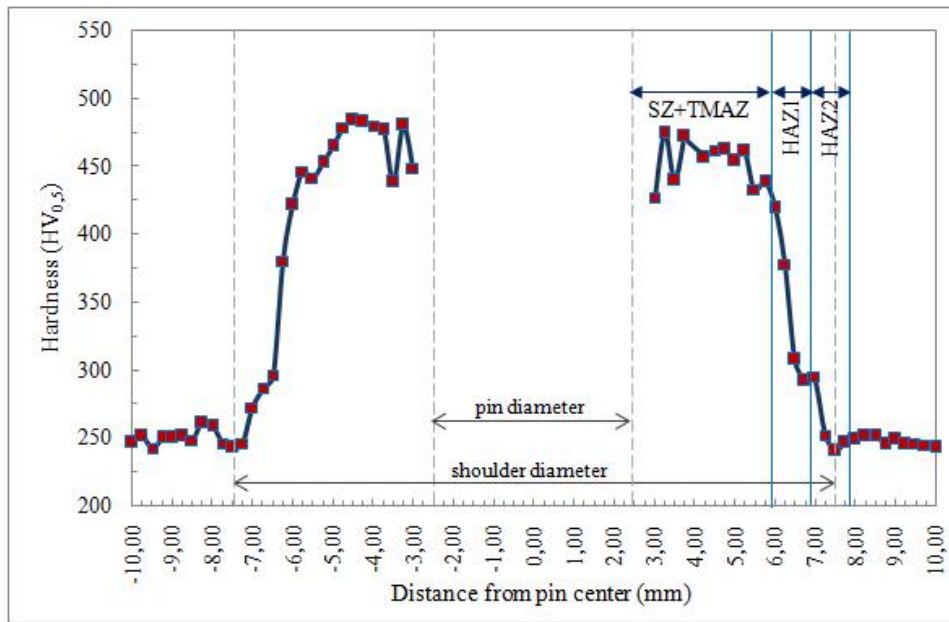
Figure 9. Microhardness profile across the weldment. Sizes of the different zones formed during the process are also indicated, as well as pin and shoulder diameters.

The average peak load value for the joints tested in lap-shear was (4.72 ± 0.83) kN. As for FSSW there is no a standard with minimum recommended values, it was compared to the minimum recommended for joints produced by resistance spot welding, according to the AWS D8.1M standard (2007), which is 5.8 kN. The resultant peak load in FSSW using the welding conditions adopted was lower than that one. It would be expected that the existence of microconstituents of low toughness, as Widmanstätten ferrite, coalesced bainite and martensite, could make the joint brittle. But the analysis at SEM showed a ductile fracture mechanism, evidenced by dimples elongated in direction of applied load, as can be observed in Fig. 10.
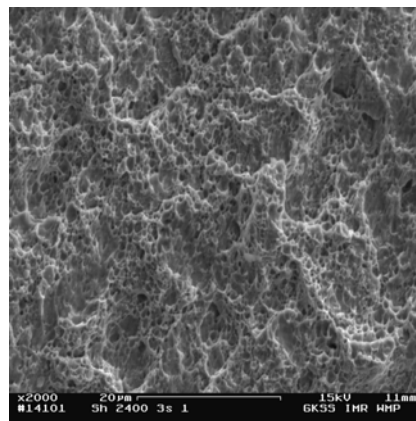
Figure 10. Fracture surface of a lap-shear sample exhibiting dimples.

The analysis of the transversal section of the fractured samples showed that fractures occurred in SZ, as showed in Fig. 11(a): they started at the interface between the sheets, that acted as a notch, and then followed the zinc line formed due to the material flow. Some secondary cracks were observed linking up the allotriomorphic ferrite produced in SZ, Fig. 11(b). This two constituents, zinc and allotriomorphic ferrite, have low resistance, so in the stir zone they were the easier path for crack propagation during lap-shear test, leading to low peak force values reached during the tests.
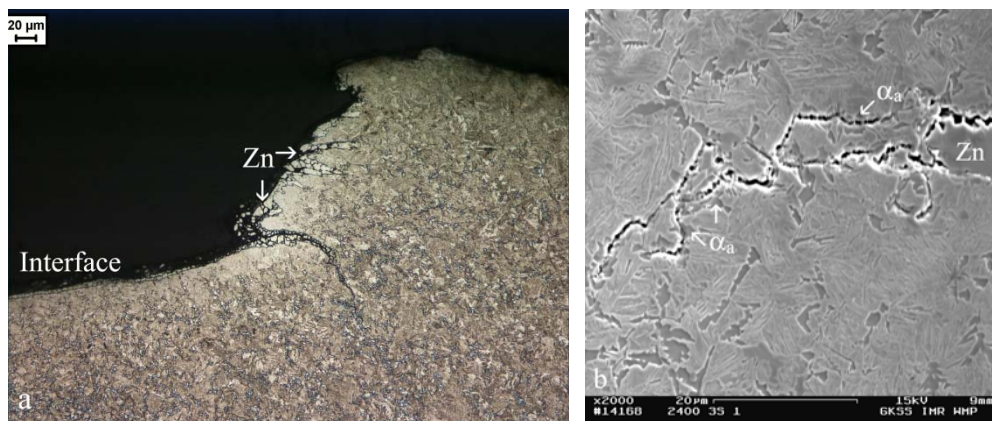
Figure 11. Transversal section of a sample fractured in lap-shear: (a) crack propagation through the zinc line (OM); (b) secondary cracks propagated in the allotriomorphic ferrite formed in SZ (SEM).

4. CONCLUSIONS

Friction stir spot welds of a TRIP 800 steel were produced using a PCBN tool. Process outputs, microstructure and properties were evaluated for a rotational speed of 2400 rpm and dwell time of 3 s. Different zones were formed during the welding process, namely stir zone, thermomechanical affected zone and heat affected zone. The high heat input employed, associated with high deformation, resulted in formation of large amount of allotriomorphic ferrite in stir zone, besides a mixture of conventional weld phases as Widmanstätten ferrite, upper bainite and martensite, as well as coalesced bainite and martensite-austenite constituent. The thermomechanical affected zone was composed by ferrite, austenite, bainite and martensite. Heat affected zone exhibited two subzones: HAZ1 and HAZ2. Whereas the microstructure in HAZ1 was ferrite and austenite, the resultant microstructure in HAZ2 was ferrite, bainitic ferrite and retained austenite. As the TRIP steel sheets used in this study had a zinc coating, after welding a zinc line was observed in stir zone. The fracture mechanism of samples tested in lap-shear was ductile. The fracture initiated at the interface between the sheets, then followed the zinc line in stir zone. Some secondary cracks also propagated along allotriomorphic ferrite in this zone. Because of this, produced joints exhibited low lap-shear strength.

5. ACKNOWLEDGEMENTS

6. REFERENCES

American Welding Society. AWS D8.1M:2007. "Specification for automotive weld quality - resistance spot welding of steel". 28p.

Bhadeshia, H. K. D. H., 1995, "Mathematical modelling of weld phenomena", Institute of Materials, London, 384 p.

Chung, J.H., Jeon, J.B. and Chang, Y.W. 2010, "Work-hardening and ductility enhancement mechanism of cold rolled multiphase TRIP steels". Metals and Materials International, Vol. 16, No. 4, pp. 533-541.

Feng, Z., Santella, M.L., David, S.A., Steel, R.J., Packer, S.M., Pan, T., Kuo, M. and Bhatnagar, R.S., 2005. "Friction stir spot welding of advanced high-strength steels: a feasibility study". SAE Technical Paper 2005-01-1248.

Furnémont, Q., Kempf, M., Jacques, P.J., Göken, M. and Delannay, F. 2002. "On the measurement of nanohardness of the constitutive phases of TRIP-assisted multiphase steels". Materials Science and Engineering A, Vol. 328, pp. 26-32.

Gerlich, A., Su, P. and North, T.H. 2005. "Friction stir spot welding of Mg-alloys for automotive applications". Magnesium Technology, pp. 383-388.

Gerlich, A., Su, P., Yamamoto, M. and North, T.H. 2008. "Material flow and intermixing during dissimilar friction stir welding". Science and Technology of Welding and Joining, Vol. 13, No.3, pp.254-264.

Girault, E., Jacques, P., Harlet, P., Mols, K., Van Humbeeck, J., Aernoudt, E. and Delannay, F. 1998. "Metallographic methods for revealing the multiphase microstructure of TRIP-assisted steels". Materials Characterization, V. 40, No. 2, pp. 111-118.

Gould, J.E., Khurana, S.P. and Li, T. 2006. "Predictions of microstructures when welding automotive advanced high-strength steels". Welding Journal, pp. 111s-116s.

Hanlon, D.N., Sietsma, J. and van der Zwaag, S. 2001. "The effect of plastic deformation of austenite on the kinetics of subsequent ferrite formation". ISIJ International, Vol. 41, No. 9, pp. 1028-1036.

Hanzaki, A.Z., Hodgson, P.D. and Yue, S. 1997. "Retained austenite characteristics in thermomecanically processed Si-Mn transformation-induced plasticity steels". Metallurgical and Materials Transactions A, Vol. 28, pp. 2405-2414.

International Organization for Standardization. ISO 14273:2000 (E). "Specimen dimensions and procedure for shear testing resistance spot, seam and embossed projection welds". 8p.

Jacques, P.J., Ladrière, J. and Delannay, F. 2001, "On the influence of interactions between phases on the mechanical stability of retained austenite in Transformation-Induced Plasticity multiphase steels". Metallurgical and Materials Transactions A, Vol. A32, pp. 2759-2768.

Jacques, P.J., Mertens, A., Verlinden, B., Van Humbeeck, J. and Delanney, F., 2001. "The developments of cold-rolled TRIP-assisted multiphase steels. Al-alloyed TRIP-assisted multiphase steels". ISIJ International, V. 41, No. 9, pp. 1068-1074.

Jacques, P.J., Furnémont, Q., Lani, F., Pardoen, T. and Delannay, F. 2007. "Multiscale mechanics of TRIP-assisted multiphase steels: I. characterization and mechanical testing". Acta Materialia, Vol. 55, No. 11, pp. 3681-3693.

Jandová, D., Bernášek, V., Paterová, H. and Kešner, D. 2004. "Microstructure and phase transformations in alloy steels and simulations of their processing". AEDS Workshop, Pilsen, República Tcheca.

Kaputkina, L.M., Morozova, T.I. and Vladimirskaya, T.K. 1986. "Structure and properties of constructional steels after high-temperature thermomechanical isothermal working". Metal Science and Heat Treatment, Vol. 28, No. 3, pp. 169-173.

Khan, M.I., Kuntz, M.L., Su, P., Gerlich, A., North, T. and Zhou, Y. 2007, "Resistance and friction stir spot welding of DP600: a comparative study". Science and Technology of Welding and Joining, Vol. 12, pp.175-182.

Kyffin,W.J., Addison, A.C., Martin J. and Threadgill, P.L., 2006a, "Recent developments in friction stir spot welding of automotive steels." Proceedings of XII Sheet Metal Welding Conference, Livinoia, Michigan.

Kyffin, W.J., Threadgill, P.L., Lalvani, H. and Wynne, B.P., 2006b, "Progress in FSSW of DP800 high strength automotive steel", Proceedings of the 6th International Symposium 'Friction stir welding', St. Sauveur, Quebeck.

Larn, R.H. and Yang, J.R. 2000. "The effect of compressive deformation of austenite on the bainitic ferrite transformations in Fe-Mn-Si-C steels". Materials Science and Engineering A, Vol. 278, No. 1-2, pp. 278-291.

Mazda, 2003. "Mazda develops world's first aluminum joining technology using friction heat". <http://www.mazda.com/publicity/release/2003/200302/0227e.html>

Mazda, 2005. "Mazda develops world's first steel and aluminum joining technology using friction heat". <http://www.mazda.com/publicity/release/2005/200506/050602.html>

Mazzaferro, C.C.P. Soldagem a ponto por fricção e mistura mecânica de um aço TRIP 800: processo, microestrutura e propriedades. Tese de Doutorado. Programa de Pós-Graduação em Engenharia de Minas, Metalúrgica e de Materiais. Universidade Federal do Rio Grande do Sul, 2008.

Ryu, H.-B., Speer, J.G. and Wise, J.P. 2002. "Effect of thermomechanical processing on the retained austenite content in a Si-Mn transformationinduced plasticity steel". Metallurgical and Materials Transactions A, pp. 2811-2816.

Samek, L., De Moor, E., Penning, J. and De Cooman, B.C. 2006. "Influence of alloying elements on kinetics of strain-induced martensitic nucleation in low-alloy, multiphase high-strength steels". Metallurgical and Materials Transactions A, Vol. 37, pp. 109-124.

Santella, M., Hovanski, Y., Frederick, A., Grant, G. and Dahl, M., 2010. "Friction stir spot welding of DP780 carbon steel". Science and Technology of Welding and Joining, Vol. 15, No. 4, pp. 271-278.

Skálová, L., Divisová, R. and Jandová, D. "Thermo-mechanical processing of low-alloy TRIP-steel". 2006, Journal of Materials Processing Technology, Vol. 175, Issues 1-3, pp. 387-392.

Srivastava, A.K., Bhattacharjee, D., Jha, G., Gope, N. and Singh, S.B., 2007. "Microstructural and mechanical characterization of C-Mn-Al-Si cold-rolled TRIP-aided steel". Materials Science and Engineering A, 2007, Vol. A445-446, pp. 549-557.

Su, P., Gerlich, A. and North, T.H., 2005. "Friction stir spot welding of aluminum and magnesium alloy sheets". SAE Technical Paper 2005-01-1255, pp.127-133.

Su, P., Gerlich, A., North, T.H. and Bendzsak, G.J. 2006a. "Energy generation and stir zone dimensions in friction stir spot weldings". SAE Technical Paper 2006-01-097, pp. 179-187.

Su, P., Gerlich, A., North, T.H. and Bendzsak, G.J. 2006b. "Energy utilization and generation during friction stir spot welding". Science and Technology of Welding and Joining, Vol. 11, No. 2, pp. 163-169.

Thomas, W.M., Nicholas, E.D., Needham, J.C., Murch, M.G., Temple-Smith, P. and Dawes, C.J., 1991. "Friction-stir butt welding". GB Patent No. 9125978.8, International patent application No. PCT/GB92/02203.

Wan, J., Chen, S. and Hsu, T.Y. 2003. "Effect of stacking fault energy and austenite strengthening on martensitic transformation in Fe-Mn-Si alloys". Journal of Physics IV, Vol. 112, pp. 381-384.

Whelan, M.J., Hirsch, P.B., Horne, R.W. and Bollmann, W. 1957. "Dislocations and stacking faults in stainless steel". Proceeding of the Royal Society of London A, Vol. 240, pp. 524–538.

Zaefferer, S., Ohlert, J. and Bleck, W. 2004. "A study of microstructure, transformation mechanisms and correlation between microstructure and properties of a low alloyed TRIP steel". Acta Materialia, Vol. 52, pp. 2765-2778.

7. RESPONSIBILITY NOTICE

The authors Cíntia Cristiane Petry Mazzaferro, José Antônio Esmerio Mazzaferro, Jorge Fernandez dos Santos and Telmo Roberto Strohaecker are the only responsible for the printed material included in this paper.